We are IntechOpen, the world's leading publisher of Open Access books Built by scientists, for scientists

4,800
Open access books available

122,000
International authors and editors

135M
Downloads

Our authors are among the

154
Countries delivered to

TOP 1%
most cited scientists

12.2%
Contributors from top 500 universities

CLARIVATE ANALYTICS BOOK CITATION INDEX INDEXED

WEB OF SCIENCE™

Selection of our books indexed in the Book Citation Index in Web of Science™ Core Collection (BKCI)

Interested in publishing with us?
Contact book.department@intechopen.com

Numbers displayed above are based on latest data collected.
For more information visit www.intechopen.com

Chapter 9

Modeling Dynamics Behaviour of Materials: Theoretical Framework and Applications

Giovanni Leonardi and Michele Buonsanti

Additional information is available at the end of the chapter

http://dx.doi.org/10.5772/50642

1. Introduction

The study of the dynamic behaviour of materials falls in a multidisciplinary area where many different disciplines converge. The definition of the state of the solid body subject to various actions is very different from the conditions of almost static load, or single dynamic load.

Complex dynamic actions (i. e. explosion, travelling waves, etc.) request an approach where both inertia and kinetics of the material are fundamental elements to describe the variable answer in terms of stress and strain.

The topics covered in the chapter are the following:

A first section, where particular attention about the shock waves-induced phase transformations and chemical changes will be given. A modelling coupled multifield processes will be introduced in the multiphase solids case through constitutive assumption, energy balance and mass transfer and a reaction-diffusion model.

A second part in which some applications of finite element analysis to multi-physics dynamic problems is presented and discussed.

2. Waves equations

When an elastic media is subject, over one or more points, to fast actions then media acceleration results. The strain field resulting is carried out within the media by elastic waves, and so the new and variable stress field should be equilibrated [1, 2].

Let us call u the displacement field, λ and μ the Lamè elastic constants, ρ the media density then, in the isotropic, homogeneous and elastic media we have the follow motion equation:

$$\rho ii = \mu \nabla^2 u + (\lambda + \mu)\nabla(\nabla u) \tag{1}$$

In the Eq. (1) the symbol ∇ represents the nabla differential operator. Under the volume forces equal to zero one possible solution to the Eq. (1) has the form:

$$u(x,t) = u(t - nx / c) \tag{2}$$

where n is a constant unit vector and c represents the velocity. Representing the Eq. (2) the solution to the Eq. (1) we observe that the Eq. (2) is a plane wave equation scattering in n direction, with c velocity. When a direction is fixed, for example x_1, then we have:

$$u(x,t) = u[t - (x_1 / c)] \tag{3}$$

Generally, an elastic wave can be of two kinds, longitudinal (volume wave) or transversal (shear wave), and respective velocities go with the function:

$$\alpha = sqr[(\lambda + 2\mu) / \rho]; \qquad \beta = sqr(\mu / \rho) \tag{4}$$

As a principle, we have an elastic wave's emission when a fast, and localized variation on the body force exists.

In this case, the Eq. (1) appears as a Green tensor, that is a second order tensor time dependent, G_{ij} (x, t; ε, τ). Neglecting isotropic source, the dynamics source gives out longitudinal and transversal waves with various amplitude according to the direction.

The wave shape represents the signal shape reproduced by the source, in other words the temporal course of the source namely, the $F(t)$ function.

Since the Green tensor calculation appears with difficulty, through known references, it becomes possible to proceed by the Helmholtz potential method, and therefore to derive, for convolution, the Green tensor final form [3]:

$$\begin{aligned} G_{ij}(x,t;0,0) &= (1/4\pi\rho)(3\gamma_i\gamma_j - \delta_{ij})r^{-3}t[H(t - r^{\alpha^{-1}}) - H(t - r\beta^{-1})] + \\ &+[(1/4\pi\rho\alpha^2)\gamma_i\gamma_j\delta(t - r\alpha^{-1})] + [(1/4\pi\rho\beta^2)(\delta_{ij} - \gamma_i\gamma_j)\delta r^{-1}(t - r\beta^{-1})] \end{aligned} \tag{5}$$

Where γ_i and γ_j are the director cosine of x, δ the x varied position and δ_{ij} the Kronecker delta.

The Eq. (5) is composed by 3 terms, all depending on the distance. We have the first one, called close field, while the other two called away fields. We observe not separable waves in the close field while, in the away field longitudinal and transversal waves appear distinct. All of this allows, in the next modelling to consider only the close field and then longitudinal and transversal motions together.

Here we consider plane waves travelling in an elastic half-space and, without loss of generality, we affirm that the wave normal lies in the vertical plane of the half-space. Referring to the infinite space case, we assume that the particle motion, due to dilatational

effects, belongs to the wave normal direction and therefore lies in the vertical plane. Otherwise, the particle motion, due to shear effects, present components in either vertical or horizontal plane. Introducing the functions H and Φ, called the Helmholtz potential functions, the governing equations related on this approach follow:

$$\begin{aligned} u_x &= (\partial\Phi / \partial x) + (\partial H_z / \partial y); \quad u_y = (\partial\Phi / \partial y) + (\partial H_z / \partial x); \\ u_y &= (\partial H_z \partial y) + (\partial H_y / \partial x); \quad (\partial H_x / \partial x) + (\partial H_y / \partial x) = 0. \end{aligned} \tag{6}$$

The stress-displacement relations are given by:

$$\begin{aligned} \sigma_{xx} &= (\lambda + 2\mu)[(\partial^2\Phi / \partial x^2) + (\partial^2\Phi / \partial y^2)] - 2\mu[(\partial^2\Phi / \partial y^2) - (\partial^2\Phi / \partial x^2) - \partial^2 H_x / \partial y \partial x)] \\ \sigma_{yy} &= (\lambda + 2\mu)[(\partial^2\Phi / \partial x^2) + (\partial^2\Phi / \partial y^2)] - 2\mu[(\partial^2\Phi / \partial y^2) - (\partial^2\Phi / \partial y^2) - \partial^2 H_x / \partial y \partial x)] \\ \tau_{xy} &= \mu[2(\partial^2\Phi / \partial x \partial y) + (\partial^2 H_z / \partial y^2) - (\partial^2 H_z / \partial x^2)] \\ \tau_{yz} &= \mu[2(\partial^2 H_x / \partial^2 y) + (\partial^2 H_y / \partial y \partial x)] \end{aligned} \tag{7}$$

Moreover at Eq. (7) the boundary conditions should be summed:

$$\sigma_{yy} = \tau_{yx} = \tau_{yz} = 0; \qquad y = 0 \tag{8}$$

In according with [5], we see that the problem above defined can be uncoupled and therefore resolve the motion problem into two parts, namely the first one is plane strain, such that $u_z = 0$, u_x, $u_y \neq 0$. The second one is the secondary wave motion where only $u_z \neq 0$.

From now on, we wish to study the interaction of elastic waves with discontinuities or boundaries of more complex shape than that of the half-space framework.

Particularly, we focus the attention over the scattering of compression waves against absorbed obstacles [3, 5], as well as inclusion, in elastic half-space. The propagation and reflection of waves, generated by dynamical forcing over the external surface, against inner surfaces or discontinuity [4-6] has, also, great interest in seismology, structural foundations since the vibratory phenomenon represents a very important further load condition for global stability and strength [7-9].

Moreover this building framework picks up more general problems, for example voids, flaws or stress raise in half-space constituent materials. The approach adopted follows the stated assumptions and hypothesis , that is expansion of the wave fields in series.

3. Shock waves

The impact between two solid elements represents the simplified condition for the generation of shock waves. In the specific case of parallel impact the two surfaces enter in contact simultaneously and all the points of the two surfaces enter in contact at the same time.

The true profile of a shock wave is complex. In the following Figure 1, it is possible to observe the difference between the ideal and the true profile where, for the latter, it is clear the dependence form the characteristics of the material and the pressure applied at contact.

An impulsive stress on contact has an initial, middle and final pressure value. Initially it's a shock wave (discontinuity in compression); the mean reaction is characterized from a slow variation of pressure and the final from a dissolution which tends to the undisturbed state.

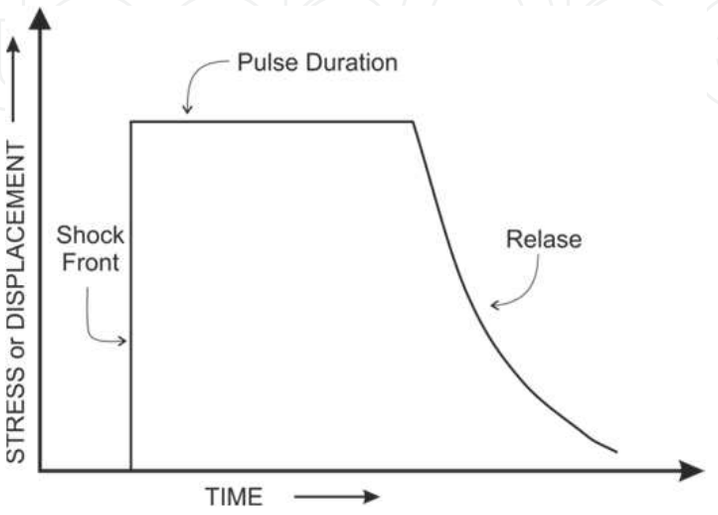

Figure 1. (*a*) idealized and *(b)* generic realistic shock wave profile (from Meyers [10]).

In a previous paper the authors has investigated the waves generation after the impact on a granular plate [9]. The study has been developed, initially from a microscopic point of view and subsequently on macroscale.

The effects are strictly linked with material degradation associated with damage evolution. In accordance to [11] the shock waves can induce phase transitions in the solid, (Figure 2), then transitions form elastic to plastic response (in our case plasticization of the mixture binding component).

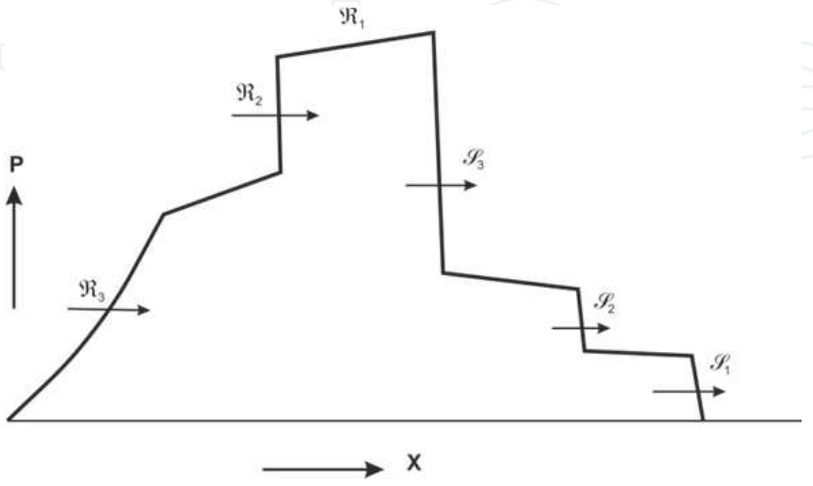

Figure 2. Pressure distribution in a pulse propagating through a material undergoing a phase transformation and a transition from elastic to inelastic behaviour (from Meyers [10]).

On a theoretical point of view, we classify the problem as the propagation of a shock wave, where a uniform contact pressure is applied on a plane solid surface in an elastic semi space. Given the geometrical origin $x = 0$ and the beginning of the phenomenon at time $t = 0$, after a laps of time t the shock front divides the space in two regions, one undisturbed, the other compressed and accelerated. Therefore the flow equation is reduced to the jump condition:

$$\Delta P = \frac{(v_s - v_o)(v_p - v_s)}{V_s} \tag{9}$$

with v_s the wave propagation speed, v_o and v_p are the speeds of the particles respectively behind and in front of the shock front, and, V_s is the specific volume of the medium.

The clear result is the introduction of a pressure step which travels across the medium, with changes of shape which depend on the mechanical proprieties of the element.

In the case of impact the contact time tends to zero, therefore $t_i = t_p$ where t_i is the impact time and t_p is the plasticization time. In theory, the problem can be represented as two successive phases.

First phase: transversal speed at the centre of the body remains constant. This phase is necessary to absorb the remaining kinetic energy in the body.

Second phase: a concentrated plasticization begins which starts to expand from the core to the external part of the body. The time it takes is given by the expression:

$$t = \mu v^o r^2 / 6M^o \tag{10}$$

Where μ is the Lame's material constant and the associated maximum permanent transversal displacement in the contact zone can be approximated as:

$$\omega \cong 3p_0^2 r^2 / 4\mu p_c \tag{11}$$

In regards to the mechanical proprieties of the medium subject to the impact actions in the case, the response of solids made of asphalt mixtures can be divided, accordingly to [12, 13] in three groups: elastic visco-elastic and visco-plastic. In the one-dimensional case we have:

$$E_{ii}^e = \epsilon^{-1} T_{ii} \tag{12}$$

$$E_{ii}^{ve} = A(T_{ii}) t^{\alpha} \tag{13}$$

$$E_{ii}^{vp} = B(T_{ii}) f(N) t^{\beta} \tag{14}$$

where $f(N)$, $A(T)$, $B(T)$ are functions of the stress in the viscose phase. A, B, α, β and ε are constants determined at constant temperature.

In the multidimensional case the equations above become:

$$[E]^{e} = [K]\cdot[T] \tag{15}$$

$$[E]^{ve} = At^{\alpha}[H]\cdot[T^{h}] \tag{16}$$

where K is the deformability matrix, $H = \epsilon K$ and $T^{h} = [T_{ijk}]T$

In regard to the visco-elastic part, it has to be specified that the critical points which arise in this phase with the load time can be resolved using the Perzyna theory [13]. For an associated visco-plastic flow we have:

$$[E]^{vp} = \gamma\cdot\phi(t)\cdot\partial F / \partial t \tag{17}$$

where:

- γ is a fluidity parameter associated to the loading times and the number of loading cycles;
- ϕ(F) is the viscose flow function;
- F is the plasticity function $F(T, k)$ with k the hardening parameter.

Passing to the numerical implementation, in the case of reduced load intervals, an iterative procedure, as a Newton-Raphson, can be applied.

$$A[T]^{n} = [K][A[E]]^{n} - A\alpha t^{\alpha-1}[K][T^{h}]^{n} - A[E^{vp}]^{n} \tag{18}$$

and, after the rightful developing, stress and strain in approximated as:

$$[T]^{n-1} = [T]^{n} + A[T]^{n} \tag{19}$$

$$[E^{vp}]^{n+1} = [E^{vp}] + A[E^{vp}]^{n} \tag{20}$$

Therefore it follows the link between micro-scale effects and material behaviours at macro-scale.

So we focus the micromechanics of the damage processes because the nonlinear response of typical engineering materials is almost entirely dependent on the primary change in the concentration, distribution, orientation and defects in its structural composition.

The relation between the continuum damage mechanics and the fracture mechanics is very complicated, in essence, a question of scale. The important role of scale can be clarified by an energetic point of view.

In view of an approximated continuum theory with the physical foundation of micromechanical models, a promising strategy would consist of combining the best features of both models. In this approach we consider only the first layer of the pavement package because, at micro-scale, damage distribution at the edge of the body, where surface degradation is of importance, is expected to be significantly different from the damage distribution far from the edge in the body.

We follow the volume element theory RVE, it's possible to represent a non-homogeneous solid with periodic microstructure. Particularly in the transition toward the micro-scale our RVE can be represented by more granular elements joint by means of an asphalt mixture, so considerations are applied on the contact area among two granular elements. In this manner the homogenization problems can be satisfied.

Following Sneddon's solution [14] type we model the physics of impact by means of a rigid frictionless asymmetric concentrated impact, with generic concave profile described by the function $f(r)$. We find respectively, the σ_z pressure distribution under the concentrated impact and the displacement on the surface.

4. Shell structures and blast loading

To reproduce a possible genuine model becomes fundamental to describe the single load conditions since blast action, fundamentally, can be decomposed in thermal and shock wave's loads. Here we develop the theoretical assumptions in both cases just starting with some structural considerations about the thick shell behaviour.

From a structural point of view the tunnel can be considered as well as a half thick-walled cylinder subject to internal and external pressures. So we consider a half cylinder of inner radius a and outer radius b and subject to an internal pressure p_a and an external pressure p_b. We choose, as the closest to real behaviour, the plane stresses condition so that the ends of the cylinder be free to expand.

Assuming the z-axis as the revolution axis, the deformation becomes symmetrical respect to the z-axis. Consequently it's convenient to use cylindrical coordinates r, θ, z.

According to [16-18] the plane stresses conditions involve $\sigma_z = 0$ and $\tau_{rz} = 0$ and the equilibrium conditions, without body forces become.

$$\frac{\partial \sigma_r}{\partial r} + \frac{\sigma_r - \sigma_\theta}{r} = 0 \tag{21}$$

while the deformation field E as the components in the form:

$$E_\theta = \frac{1}{r}\frac{\partial u_\theta}{\partial \theta} + \frac{u_r}{r}; \quad E_r = \frac{\partial u_r}{\partial r}; \quad E_r = \frac{\partial u_z}{\partial z} \tag{22}$$

where the function $u(r, \theta, z)$ represents the displacements field over the shell.

Introducing the Lame's constitutive equations (with ν and ε, respectively, Poisson's and Young's modulus) after some simple calculations we get the basic equations governing the thick-walled half-cylinder:

$$u_r = \frac{1-\nu}{\epsilon}\frac{p_a a^2 - p_b b^2}{b^2 - a^2} r + \frac{1+\nu}{\epsilon}\frac{a^2 b^2}{r}\frac{p_a - p_b}{b^2 - a^2}$$

$$\sigma_r = \frac{p_a a^2 - p_b b^2}{b^2 - a^2} - \frac{b^2 a^2}{r^2}\frac{p_a - p_b}{b^2 - a^2}$$

$$\sigma_\theta = \frac{p_a a^2 - p_b b^2}{b^2 - a^2} + \frac{b^2 a^2}{r^2}\frac{p_a - p_b}{b^2 - a^2} \tag{23}$$

Under these conditions, we recall either of the specific conditions of the internal and external pressure loads. In the first case (internal pressure) the above equations becomes:

$$\begin{aligned} \sigma_r &= \frac{p_a a^2}{b^2 - a^2}\left(1 - \frac{b^2}{r^2}\right) \\ \sigma_\theta &== \frac{p_a a^2}{b^2 - a^2}\left(1 + \frac{b^2}{r^2}\right) \end{aligned} \tag{24}$$

From the equations above, a consideration can be drawn about the circumferential stress (σ_θ tensile stress), which is at its greatest on the inner surface and is always greater than p_a. In the second case (external pressure) the general equations assume the form:

$$\begin{aligned} \sigma_r &= -\frac{p_b}{b^2 - a^2}\left(1 - \frac{a^2}{r^2}\right) \\ \sigma_\theta &= \frac{p_b b^2}{b^2 - a^2}\left(1 + \frac{a^2}{r^2}\right) \end{aligned} \tag{25}$$

The stress paths, when no inner holes were present, are uniformly distributed in the cylinder. From now we will be able to describe the coupling actions over the thick-walled half-cylinder shell and for this we run recalling some basic thermo-elasticity assumption. There is a large literature over the question but we prefer to follow [18-20].

We focus the consistence of thermal stresses induced in thick-walled half-cylinder when the temperature field is symmetrical about the z-axis. In this case we suppose the temperature T as radius function only and independent from z then plane strain $E_z = 0$. With analogous considerations as above, the basic equations, for the coupled problem, can be written as.

$$\begin{aligned} u_r &= \frac{(1+\nu)\alpha}{(1-\nu)r}\left\{\int_a^r Trdr + \frac{(1-2\nu)r^2 + a^2}{b^2 - a^2}\int_a^b Trdr\right\} \\ \sigma_r &= \frac{\alpha\epsilon}{(1-\nu)}\frac{1}{r^2}\left\{\frac{r^2 - a^2}{b^2 - a^2}\int_a^b Trdr - \int_a^r Trdr\right\} \\ \sigma_\theta &= \frac{\alpha\epsilon}{(1-\nu)}\frac{1}{r^2}\left\{\frac{r^2 - a^2}{b^2 - a^2}\int_a^b Trdr + \int_a^r Trdr - Tr^2\right\} \\ \sigma_z &= \frac{\alpha\epsilon}{(1-\nu)}\left\{\frac{2}{b^2 - a^2}\int_a^b Trdr - Tr\right\} \end{aligned} \tag{26}$$

If the temperature T is positive and if the external temperature is equal to zero then the radial stress is always compressive, like other stresses in the inner surface.

After numerous disasters in the building and structures, the fire-structure question was developed for many researchers, which has reproduced a large and specific literature. For instance it is our opinion, referring at some as important in [16-19]. From now we will deepen the other coupled action namely the structural effects after the burst. According to [10] the interaction of a detonating explosive with a material in contact with it or in close proximity is extremely complex, since it evolves detonation waves, shock waves, expanding gases, and their interrelationships.

The question was developed, principally, by military requirement which study has developed the computational apparatus, for instance the Gurney equation [25-26].

It's our interest some basic assumption linked to the effective problem that requires us namely, only actions from shock waves. So, we affirm the following basic assumptions:

a. A shock is a discontinuous surface and has no apparent thickness.
b. The shear modulus is assumed to be zero and so it responds to the wave as a fluid, and the theory can be restricted to higher pressures.
c. Body forces and heat conduction at the shock front are negligible.
d. There is no elastic-plastic behaviour.
e. Material do not undergo phase transformations.

Now we will consider the dynamic behaviour of thick-wall cylindrical shell under internal pressure produced by shock wave.

Let p_c be the collapse pressure, then the shell is subject to a symmetrical internal pressure pulse, in the interval time $0 \le t \le \tau$, while $p = 0$ when $t \ge \tau$. Again we assume a perfectly rigid plastic material behaviour.

Supposing the pressure load symmetric, then the yielding is controlled by force in the shell middle plane. So, let N_θ be the generalized membrane forces, at the yielding point we have $N_\theta = N_c$ (with N_c the fully plastic membrane forces). Neglecting the elastic effects, the dynamics response consist of two phases motion with $N_\theta = N_\phi = N_c$.

For major clarify we consider, as the second phase, the time as $\tau \le t \le t^*$ where t^* is the response duration time. Let ω be the transverse displacement of the shell middle plane and let v° be the spherically symmetric outwards impulsive velocity, we then find the radial displacement

$$\omega = N_c t^2 / \mu r - v^o t \tag{27}$$

After some calculations we have the associated permanent radial displacement field over the shell.

$$\omega_f = -\mu r v^o / 4N_c \tag{28}$$

5. Applications examples

In the following, we will give two examples of finite element applications to dynamic analysis in particular, interaction problems of structures systems subject to explosion waves and impact loads are presented [9] [15].

5.1. Impact loads on flexible pavement

In this example we assessed the effects of a heavy impact caused by aircraft landing gear wheels on a flexible airport pavement.

Flexible pavements are usually idealized as closed systems consisting of several layers; so the surface, base, sub-base and sub-grade material were modelled using 3-D finite elements. While an elastic constitutive model was assumed for the granular layers and the base course, a time hardening creep model was incorporated to simulate the viscoelastic behaviour of the HMA surface layer

The aircraft considered in the model was the Airbus 321 [26]. The most common way of applying wheel loads in a finite element analysis is to apply pressure load to a circular or rectangular equivalent contact area with uniform tyre pressure [27]. To investigate the impact simulation in exceptional condition, the dynamic parameters of an "hard" landing, that caused the broken of some gear components, were considered [28]. Starting from this, considering the damping effect of the gear system, it is possible to calculate the acceleration graph during the landing (Figure 3).

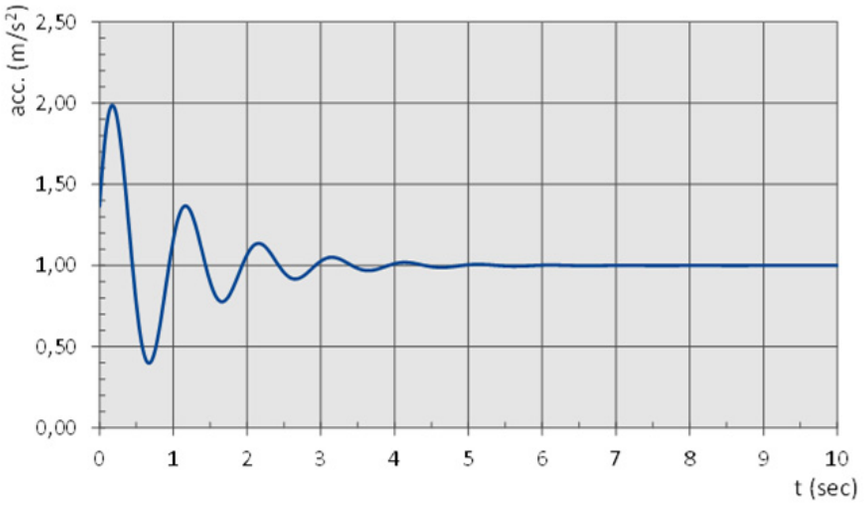

Figure 3. Acceleration graph.

As shown in Figure 3 the peak acceleration value, during the hard landing, is 1.99 m/s². This value of acceleration was used in the finite element model to calculate the maximum wheel load.

The finite element model has the following dimensions: 10 m in x and y directions and 2.5 m in the z- direction. The three-dimensional view of finite element model is shown in Figure 4.

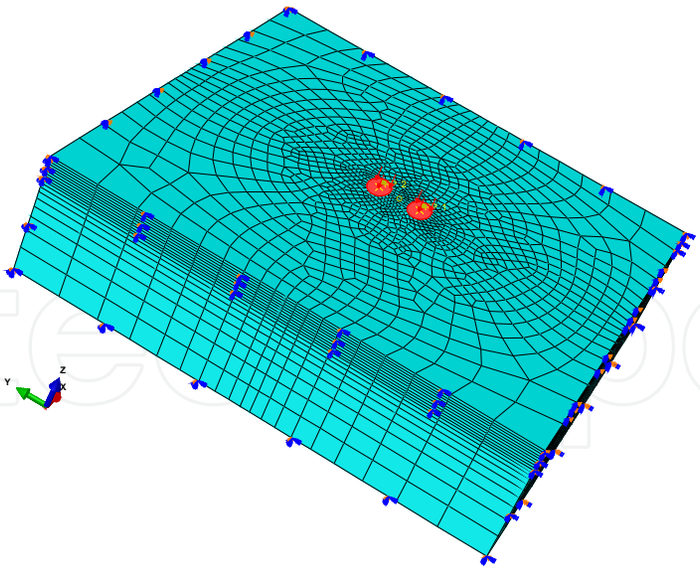

Figure 4. Three-dimensional view of the finite element model.

The degree of mesh refinement is the most important factor in estimating an accurate stress field in the pavement: the finest mesh is required near the loads to capture the stress and strain gradients. The mesh presented has 126245 nodes and 29900 quadratic hexahedral elements of type C3D20R (continuum 3-dimensional 20 node elements with reduced integration). Quadratic elements yield better solution than linear interpolation elements [29].

The loads (vertical and horizontal) were uniformly applied to the element, which was created to be the same size as the wheel imprint of an Airbus A321.

In this example the surface was considered to be free from any discontinuities (with no cracks) or unevenness, and the interface between layers was considered to be fully bonded (with no gaps).

The model was constrained at the bottom (encastre: U1 = U2 = U3 = UR1 = UR2 = UR3 = 0); X-Symm (U1 = UR2 = UR3 = 0) on the sides parallel to y-axis; and Y-Symm (U2 = UR1 = UR3 = 0) on the sides parallel to x-axis.

The results of the non-linear FE analysis are illustrated in the following figures. Figure 5 shows the Mises stress distribution for the considered FE model at the landing aircraft impact instant and Figure 6 presents the results of pavement surface deflection along transversal direction.

Finally, in the graph of Figure 7 are plotted the predicted transversal surface deflection profiles along the transverse center line.

This example shows how finite element analysis of pavement structures, if validated, can be extremely useful, because it can be used directly to estimate pavement response parameters without resorting to potentially costly field experiments.

If accurate correlations between the theoretically-calculated and the field-measured response parameters can be obtained, then the finite element model can be used to simulate

pavement response utilizing measurements from strain gages. In particular, the proposed model has clearly confirmed the need and importance of 3-Dimensional finite element analyses on flexible pavements to consider the behaviour of the structure under high stress.

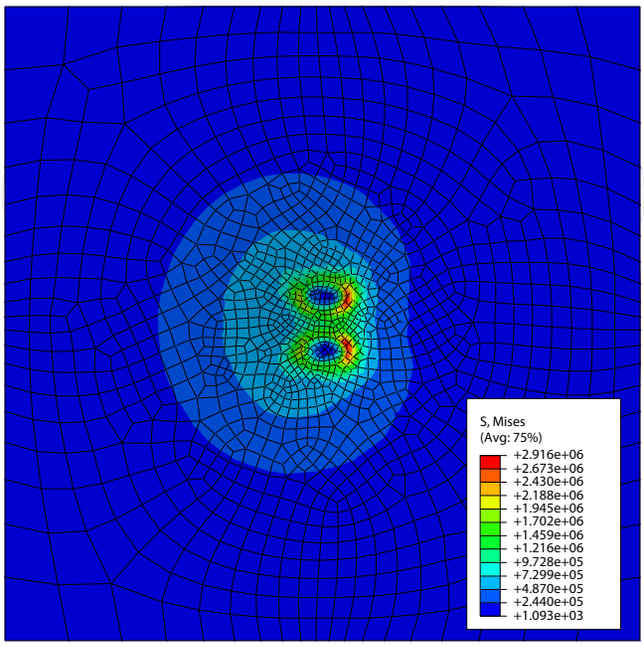

Figure 5. Mises stress at the instant of impact.

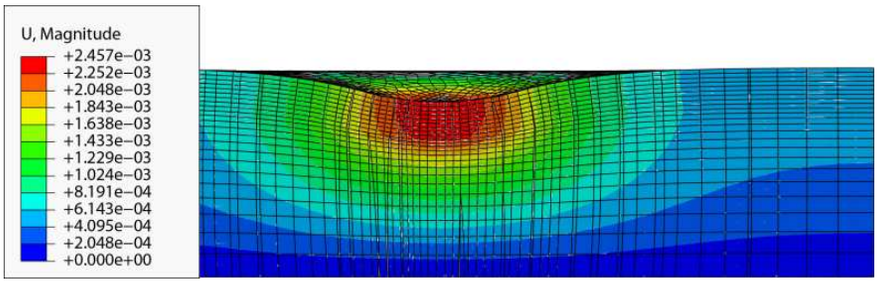

Figure 6. Displacement contours at the instant of impact.

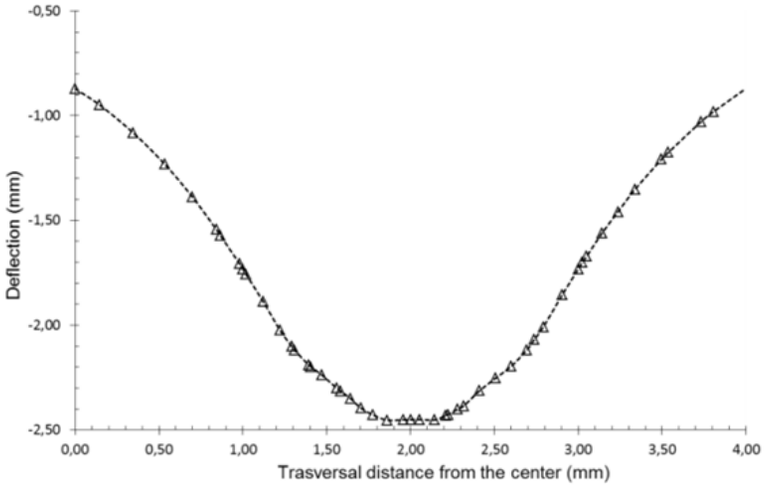

Figure 7. Predicted deflection profiles (y-direction).

5.2. Confined explosions

In the following application a 3-D simulation of tunnel structures under Blast loading is proposed.

The Finite Element model was based on a single track railway tunnel system consisting of concrete tunnel tube with the section dimensions reported in Figure 8. The tunnel was about 10 m below the ground surface. The model extended 150 m in the longitudinal direction of the tunnel, while the length and height of the model were of 26.8 m. The finite Element model was fixed at the base and roller boundaries were imposed to the four side. The modelled tunnel structure is surrounded by soil and this load represents the starting state of stress. Drucker-Prager elasto-plastic model was used to model the soil. For the characterization of the reinforced concrete of the tunnel structure it was considered a C50/60 class concrete having thermal characteristics according with the indications of the Eurocode 2 [30].

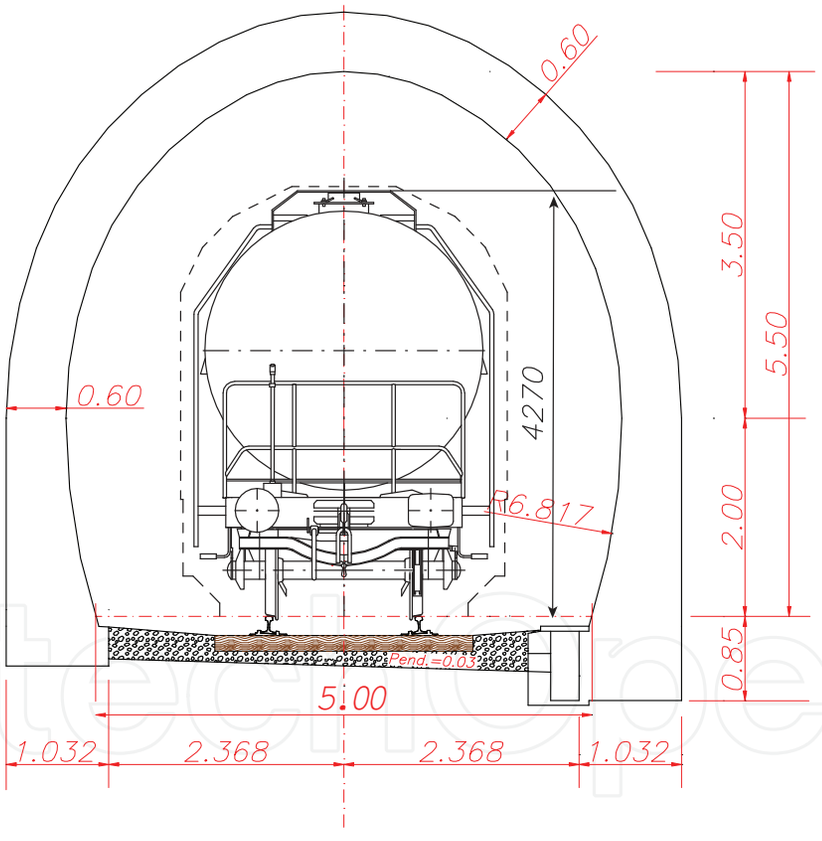

Figure 8. Rail tunnel section.

A fundamental aspect in the study of fire resistance in underground structures is the definition beforehand of the fire scenario taken in the analysis, therefore choosing the best fit standard curve. A standard curve is the cellulose curve defined in several standards, e.g. ISO 834 [23]. Specific temperature curves have been developed in some countries to simulate hydrocarbon fires in tunnels. Examples of such curves are the RABT/ZTV Tunnel Curve in Germany [31] and the Rijkswaterstaat Tunnel Curve (RWS curve) in The Netherlands (based

on laboratory scale tunnel tests performed by TNO in 1979 [32]). In the considered model the HC curve was used to simulate the fire action.

The blast overpressure was generated from an instantaneous release of 50 m^3 LPG rail tanker at 326K. The pressure-time curve was assumed to be of triangular shape, the duration of which was obtained from CONWEB reflected pressure diagram [33]. To calculate the decay of blast overpressure during the longitudinal direction of the tunnel the Energy Concentration Factor (ECF) method was used [34].

During the propagation of the blast wave over the first 75 m from the BLAVE to the tunnel opening, the blast overpressure falls from 1700 kPa (vapor pressure at 326 K) down to approximately 86 kPa. This decay is solely through the intense energy dissipation in the strong leading shock of the blast wave.

The 3-Dimensional model is representative of a tunnel section 300 meters long. This model was implemented by quadratic tetrahedral type elements [31] obtaining 95003 elements and 147528 nodes as shown in Figure 9.

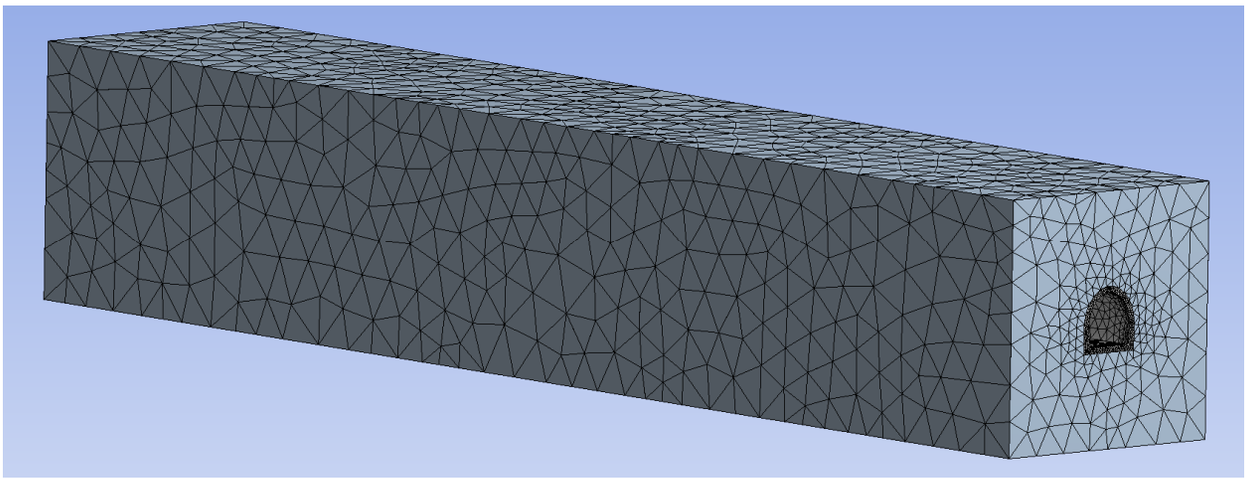

Figure 9. Meshed model.

The analysis was carried out in two steps [35]. The first step obtained the initial stress state caused by soil load and fire and the second step analysed the dynamic response under blast loading. Consequently the following load conditions were considered in the FE analysis:

1. from time $t = 0$ to time $t = 120$ min the tunnel was subjected to the surrounding soil load and to the fire thermal stress;
2. at the instant $t = 2$ sec the structure was subjected to the blast over pressure.

Therefore, on the base of this analysis, the distribution of the temperature inside of the structure is known. In Figure 10 the temperature distribution is showed.

Subsequently, the mechanical behaviour of the models was analysed introducing also to thermal stress, the explosion load. Figure 11 shows the deformation and the Mises stress of tunnel section, from meddle, where explosion is localized, to the tunnel opening.

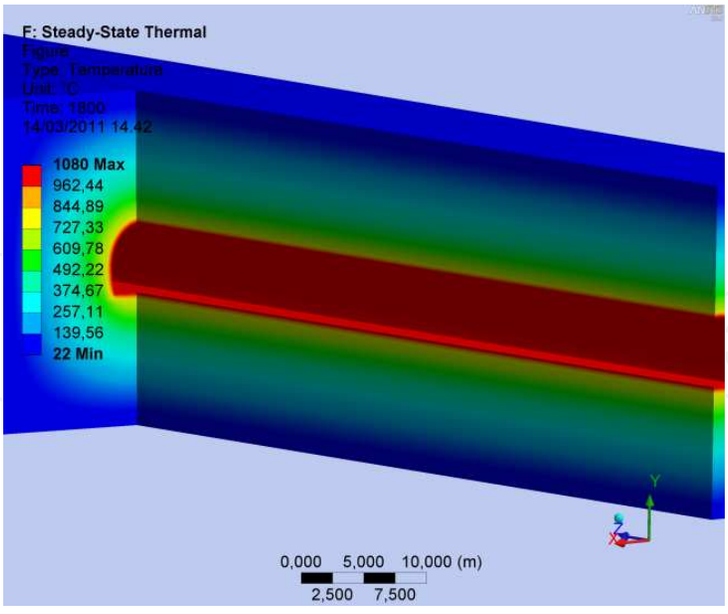

Figure 10. Temperature distribution (°C) t = 1800 sec.

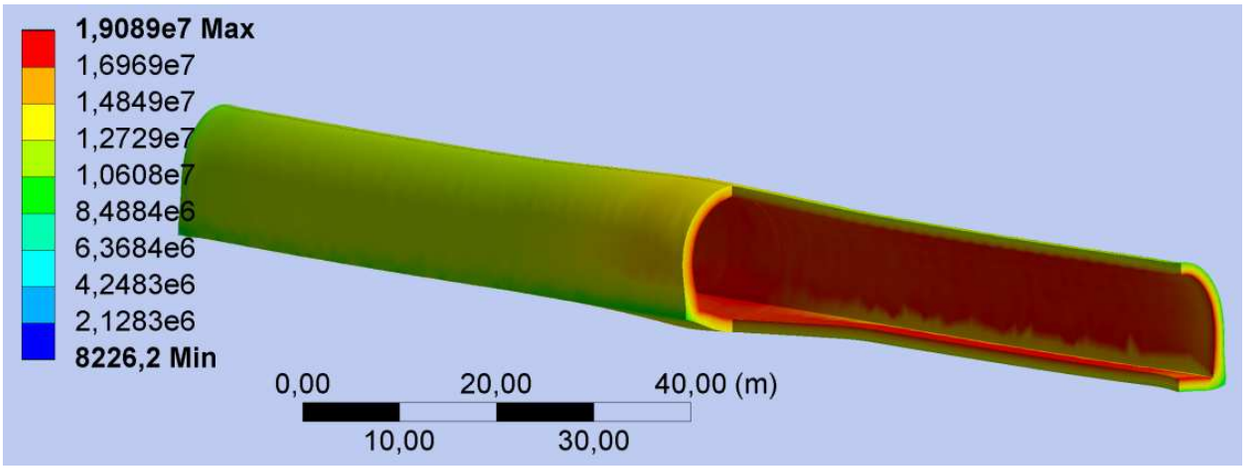

Figure 11. Mises stress (Pa) of the tunnel at the explosion instant.

6. Conclusions

The topics developed in this chapter belong to multi-physics problems and consequently represent a great computational weight on the results. Again, further complexities arise in the hypothesis of the mechanical process being dynamic.

In the almost static case the strain, in any instant of time, is in a situation of almost equilibrium with the loads; instead in the dynamic case the stress state is variable in space, therefore there are portions of the solid under stress against others in almost absence of stress. In other words the stress travels inside the solid as a stress-wave and it becomes a fundamental parameter for the description of the behaviour of the material. The dynamic processes in materials involve different scientific disciplines and areas, as materials science, shock physics/chemistry, mechanics combustion, applied mathematics and large scale computation.

Certainly, in developing this approach we have had the opportunity to deepen analysis about strength of materials and structures, and damage and fracture at micro and macroscale.

In the second section of the chapter, two numerical simulations relatively to one impact against air field pavements and one explosion in tunnel structures have been presented. Both simulations assume the problems as multi-field, and the results are quantitatively adequate.

Author details

Giovanni Leonardi* and Michele Buonsanti
Faculty of Engineering, University of Reggio Calabria,
Department of Mechanics and Materials – MECMAT, Reggio Calabria, Italy

7. References

[1] Buonsanti M., Cirianni F., Leonardi G. Study of the barriers for the mitigation of railway vibrations. In: ICSV16 Proceedings 16th International Conference of Sound and Vibrations, 5-9 July 2009, Kracòw, Poland; 2006.
[2] Truesdell C. Mechanics of Solids Waves in Elastic and Viscoelastic Solids, vol. IV, Springer-Verlag Berlin; 1984.
[3] Hudson J. A. The Excitation and Propagation of Elastic Waves, Cambridge University Press, Cambridge; 1988.
[4] Love A. E. H. A Treatise on the Mathematical Theory of Elasticity, IV Ed., Dover Pbs. New York; 1972.
[5] Graff K. F. Wave Motion in Elastic Solids, Dover Pbs. New York; 1991.
[6] Wood R. D. Diffraction of Transient Horizontal Shear Waves by a Finite Rigid Ribbon. International Journal of Engineering Science. 1970; 8: 857-874.
[7] Wood R. D., Pao Y.H. Diffractions and Horizontal Shear Waves by a Parabolic Cylinder and Dynamic Stress Concentration. Journal Applied Mechanics. 1966; 33: 785-792.
[8] Woods R. D. Screening of Surface Waves in Soils, Journal of the Soil Mechanics and Foundations Division. ASCE. 1968; 94: 951-979.
[9] Buonsanti M., Cirianni F., Leonardi G., Scopelliti F. Impact on Granular Plate. In: De Roeck G., Degrande G., Lombaert G., Muller G. (eds.) Eurodyn2011: proceedings of the 8th International Conference on Structural Dynamics, EURODYN2011, Leuven, Belgium, 2011.
[10] Meyers M. Dynamic behavior of materials. Wiley-Interscience; 1994.
[11] Duvall G., Graham R. Phase transitions under shock-wave loading, Reviews of Modern Physics. 1977; 49:523-579.

* Corresponding Author

[12] Lu Y., Wright P. Numerical approach of visco-elastoplastic analysis for asphalt mixtures, Computers & Structures. 1998; 69: 139-147.
[13] Krishnan J., Rajagopal K. On the mechanical behavior of asphalt, Mechanics of materials. 2005; 37: 1085-1100.
[14] Little R. W., Keer L. Elasticity. Journal of Applied Mechanics. 1974; 41: 7.
[15] Buonsanti M, Leonardi G, Scopelliti F. 3-D Simulation of shock waves generated by dense explosive in shell structures. Procedia Engineering. 2011; 10: 1550-5.
[16] Timoshenko S, Woinowsky-Krieger S, Woinowsky S. Theory of plates and shells: McGraw-hill New York; 1959. C. Truesdell, Mechanics of solids: Springer Verlag, 1973.
[17] Sadd M. Elasticity Theory, Applications, and Numerics. 2005. Burlington, MA: Elsevier Butterworth-Heinemann..
[18] Srinath LS. Advanced mechanics of solids: Tata McGraw-Hill Publishing Company Limited; 2009.
[19] Doghri I. Mechanics of deformable solids: linear, nonlinear, analytical, and computational aspects: Springer Verlag; 2000.
[20] Crozier DA, Sanjayan JG. Tests of load-bearing slender reinforced concrete walls in fire. ACI Structural Journal. 2000; 97(2).
[21] O'meagher A, Bennetts I. Modelling of concrete walls in fire. Fire safety journal. 1991; 17(4): 315-35.
[22] Pesavento F, Gawin D, Majorana CE, Witek A, Schrefler B. Modelling of thermal damaging of concrete structures during fire. In: VII International Conference Computational Plasticity, 2003.
[23] Schrefler B, Brunello P, Gawin D, Majorana C, Pesavento F. Concrete at high temperature with application to tunnel fire. Computational Mechanics. 2002; 29(1): 43-51.
[24] Gurney RW. The Initial Velocities of Fragments from Bombs, Shell and Grenades. DTIC Document, 1943.
[25] Kennedy J, editor. Behavior and Utilization of Explosives in Engineering Design. 1972.
[26] AIRBUS. Airplane Characteristics A321. 1995.
[27] Huang Y. Pavement analysis and design: Prentice Hall; 1993.
[28] AAIB. AAIB Bulletin: 6/2009 EW/C2008/07/02. 2009.
[29] Kuo CM, Hall KT, Darter MI. Three-dimensional finite element model for analysis of concrete pavement support. Transportation Research Record. 1995; 1505:119-27.
[30] Committee E. Eurocode2: Design of concrete structures-Part 1-2: General rules-Structural fire design. ENV 1992-1-2, 1995.
[31] Forschungsgesellschaft für Straßen - und Verkehrswesen. Richtlinien für Ausstattung und Betrieb von Tunneln (RABT). Ausgabe1985.
[32] Instituut TNO voor Bouwmaterialen en Bouwconstructies. Rapport betreffende de beproeving van het gedrag van twee isolatiematerialenter bescherming van tunnels tegen brand. Rapport B-80-33. Delft, The Netherlands 1980.
[33] Hyde D. CONWEP, Conventional Weapons Effects Program. US Army Engineer Waterways Experiment Station, Vicksburg, MS. 1992.

[34] Silvestrini M, Genova B, Leon Trujillo F. Energy concentration factor. A simple concept for the prediction of blast propagation in partially confined geometries. Journal of Loss Prevention in the Process Industries. 2009; 22(4): 449-54.
[35] Buonsanti M, Leonardi G, 3-D Simulation of tunnel structures under Blast loading. Archive of Mechanics and Engineering, in press, 2012.

IntechOpen